Design of Hierarchically Cut Hinges for Highly Stretchable and Reconfigurable Metamaterials with Enhanced Strength

Yichao Tang, Gaojian Lin, Lin Han, Songgang Qiu, Shu Yang, and Jie Yin**

Reconfigurable metamaterials[1] can switch their structures in response to external stimuli, including electric[2] and magnetic fields,[3] light,[4] heat,[5] and mechanical force,[6] and thus dynamically change their physical properties. Recently, these materials have attracted tremendous interests[7–9] owing to a wide range of potential applications, including acoustic cloaking,[10] acoustic lens,[11] wave absorber,[12] ultralight and ultrastiff metamaterials,[13] and topological protection in mechanical metamaterials.[14] Among them, the continuous structural reconfiguration induced by simple yet controllable mechanical deformation in local structure elements is of particular interest.[9,15,16] For example, by harnessing buckling instabilities in 2D and 3D metamaterials composed of periodic porous or composite structures,[6,17–19] researchers have demonstrated buckling driven pattern transformations under mechanical compression and corresponding tunable acoustic properties.[19,20] Meanwhile, there have been increasing interests in the design of stretchable mechanical metamaterials based on the concept of folding-based origami[21,22] and cutting-based kirigami.[23–25]

Recently, Cho et al.[26] illustrate the concept of generating continuous pattern transformations in a thin sheet of material by introducing designed fractal cut patterns with different motifs through rigid unit rotation. Simulations show that upon an equal-biaxial stretching strain of ≈1.8, the cut sheet could undergo extreme expandability, over 800% aerial coverage of the original area at level-6 cut. Gatt et al.[27] propose a similar concept to design a new class of hierarchical auxetic metamaterials based on the rotating rigid square units connected with hinges at vertices of squares. They simulate the auxetic behavior of a two-level idealized system.[27] The expected superior mechanical properties (e.g., extreme expandability, conformability) lie in the assumption that stretching occurs only by unit rotation without deformation of individual units in the hierarchical structures.[26] The concept of hierarchically cut structures opens a new paradigm of generating highly stretchable/compressible and tunable metamaterials, which has attracted increasing interests in design of auxetic mechanical metamaterials through different cuts and perforations,[28–31] showing great promise for wide range of applications from flexible and stretchable electronics and photonics,[32,33] to conformable electronic skin (e-skin),[34] to skin grafts, bioscaffolds, and biomedical devices.[35]

Because these concepts are rather new and the initial publications mainly focus on structural design via cutting,[26,27] the emergent mechanical behaviors contributed by the constituent material itself is yet to be examined. The discrepancy between concept and practice originates when hierarchically cut structures are modeled as a series of rigid square units connected by freely rotating hinges.[26,27,36,37] Although spring hinges appear to be a reasonable simplification for the expandable and shape-shifting behavior, the fact that real materials in the uncut marginals, i.e., hinges, where the stress concentrates, can bend and stretch, and even fail. Such issues have not been brought up with elastomeric materials that can resist tear in the prior publication.[26,27] Therefore, a physical understanding of the hierarchically cut structures' mechanical responses, including deformation mechanism and strength, is essential but remains elusive. In particular, some key questions remain to be investigated and answered. For example, upon uniaxial stretching, at which level of hierarchical cuts and which level of applied strain does the first hinge break? Can the hierarchical cut concept apply to any type of thin sheet of elastic materials even brittle materials to achieve superior properties such as shape shifting and extreme expandability? How does the localized bending or stretching deformation in the hinges globally influence the strength and robustness of the entire hierarchically cut structure? How do the constituent material properties and hierarchically cut structures contribute to the overall mechanical response? Meanwhile, it will be highly desirable to control the localized deformation in hinges with enhanced mechanical tensile strength from any type of materials (even brittle materials with ultralow tensile strength) while achieving extreme stretchability and expandability of the metamaterials.

Here, we investigate the comprehensive mechanical behaviors of hierarchically cut structures by taking into account of real constituent material properties. The mechanical response under uniaxial stretching is studied by experiments in concert

Y. Tang, G. Lin, Prof. J. Yin
Applied Mechanics of Materials Laboratory
Department of Mechanical Engineering
Temple University
1947 North 12th Street, Philadelphia, PA 19122, USA
E-mail: jieyin@temple.edu
Prof. L. Han
School of Biomedical Engineering Science and Health Systems
Drexel University
Philadelphia, PA 19104, USA
Prof. S. Qiu
Department of Mechanical Engineering
Temple University
1947 North 12th Street, Philadelphia, PA 19122, USA
Prof. S. Yang
Department of Materials Science and Engineering
University of Pennsylvania
3231 Walnut Street, Philadelphia, PA 19104, USA
E-mail: shuyang@seas.upenn.edu

DOI: 10.1002/adma.201502559

with finite element method (FEM) based numerical simulation. We demonstrate that the hierarchical cut concept can be used to design of ultra-soft materials with tailorable and nonlinear mechanical properties. The uniaxial stress–strain behavior of hierarchical metamaterials exhibits highly nonlinear and strain hardening material characteristics, as well as tunable auxetic mechanical response, which we show is the result from the deformation transition from bending-dominated to stretching-dominated deformation. We further show that this transition originates from the hierarchical structure, instead of the constituent material properties. After introduction of hierarchical cuts at Level 3, the stiffness of original continuous materials decrease by over one order of magnitude and thus the materials become extremely soft. However, severe stress concentration is found in the local region of the hinges, especially at the level 1, contributing to the ultimate structural failure. Through rational design of the local cut shape and global hierarchical hinge structures, we show enhanced extreme expandability and high tensile strength in both hyperelastic and brittle materials. Further, simply by inputting the mechanical strain, we demonstrate dynamic tuning of the phononic bandgaps of the hierarchical metamaterials.

As seen in **Figure 1**a, by introducing three orthogonal line cuts in a thin square sheet (hierarchical level of 0, i.e., LVL 0), the latter is discretized into four square units connected through four hinges at the corners with the same marginal width, i.e., the same hinge width, generating an expandable structure with a hierarchical level of 1 (LVL 1, Figure 1a) upon stretching. Hierarchical structures with self-similarity can be constructed by repeating the same orthogonal line cuts in each sublevel of the square units, leading to LVL 2 and LVL 3 (Figure 1a) and higher-level structures. Here, all the hinges are designed to have the same width throughout the hierarchical structures.

A thin sheet (≈2 mm thick) made from poly(dimethylsiloxane) (PDMS) elastomer with prescribed hierarchical cuts (up to Level 3) is first studied as a model system. The sheet is uniaxially stretched using an Instron tensile test machine until the structure begins to rupture, that is, the hinges begin to tear since they are the thinnest part of the sheet. The original clamped edges of the hierarchically cut PDMS thin sheet samples are modified by adding properly designed "arms" (Figure S0b, Supporting Information) to prevent the out-of-plane buckling during uniaxial stretching, which happens even at a small strain (<10%) when the cut samples are directly gripped without designed "arms" (Figure S0a, Supporting Information). In our experiment, no out-of-plane buckling was observed until the rupture of hinges with the properly designed "arms" applying to the sample edges (Figure S0b and Video S1–S3, Supporting Information). To quantitatively understand the mechanical response of the hierarchical structures and the origin of the mechanical failure at the hinges, we carry out FEM simulations with measured hyperelastic material properties of PDMS in comparison to experiments (see details in the Experimental Section). Upon uniaxial stretching, the expansion of the (sub) units via square unit rotation result in continuous pattern transformations and an auxetic behavior (Figure S1a-S1b, Supporting Information), i.e., negative Poisson's ratio, which is similar to that of periodic porous structures under compression.[38] As the stretch increases until hinge rupture, the measured Poisson's ratio increases monotonically from −1 to 0 for level 1, from −0.8 to 0.1 for level 2, and from −0.7 to 0.18 for level 3 structure (Figure S1c,d). The simulated structure reconfiguration with the stretching strain shows excellent agreement with experiments at all levels (Figure S1, Supporting Information).

The measured stress–strain curves of the hierarchically cut PDMS sheet (Figure 1b) at different cut levels all show a highly nonlinear and strain hardening behavior. At a relatively small applied strain, the bending-dominated deformation mode via "free" rotation of square units in the hinges leads to a linear elastic response and yield an ultralow stiffness with a shallow slope. We note that similar rotation-dominated linear response is found within a small strain range in the stress–strain curve of compressing 2D porous sheets with a square array of holes.[38] As the stretching strain further increases, the hinges rotate and tend to align to the direction of the applied strain. The bending-dominated deformation transits to a stretching-dominated one in the hinges for a larger strain, leading to an increased high stiffness and the steep increase of the stress–strain curve, in sharp contrast to the plateau stress–strain behavior due to buckling when compressing the 2D porous sheets beyond the critical buckling strain.[38] These two deformation modes are commonly found in the deformation of the struts units of cellular solids[39] for the design of light-weight and high strength materials. Similar "J-shaped" stress–strain response is found in a recent study on bio-inspired design of soft network composite materials to mimic the nonlinear properties of biological tissues such as human skin.[35] Compared to the composite design, however, the hierarchical cut design has more advantages due to its much simpler cut-based fabrication strategy and the employment of only a single material for potential applications in tissue engineering and biomedical devices. Numerical simulations on the stress–strain curves of the hierarchical structures show an excellent agreement with experiments at all levels in the range of medium strain <50%. Beyond that, the simulated stress–strain curves start to deviate and overestimate the stiffness for Level 2 and Level 3 structures. The deviation at the large strain could be in part attributed to the geometrical imperfections of cut shapes, where slight nonuniformity in hinge widths could affect the stress–strain curve, especially at the large strain due to the dominated hinge width stretching mechanism.

With further macroscopic stretching, a few hinges at Level 1 start to break apart (Figure S2, Supporting Information), followed by more breakage at the hinge area, and eventually the whole structure ruptures (Figure 1d). As the hierarchical level increases, stretchability and expandability are enhanced exponentially, which is demonstrated by the increased fracture tensile strain ε_f (defined at which the first hinge breaks) from $\varepsilon_{f1} = 40\%$ for Level 1 structure to $\varepsilon_{f3} = 72\%$ for Level 3.

In principal, as proposed in ref. [26] the method of hierarchical cuts could be applied to a thin sheet made from any type of materials, including both hyperelastic materials (e.g., PDMS) and brittle materials, to achieve large flexibility and expandability. However, when the same hierarchical cuts are applied to brittle material such as Acrylics, unlike the hyperelastic PDMS, the cut concept fails to achieve the ideal expandability

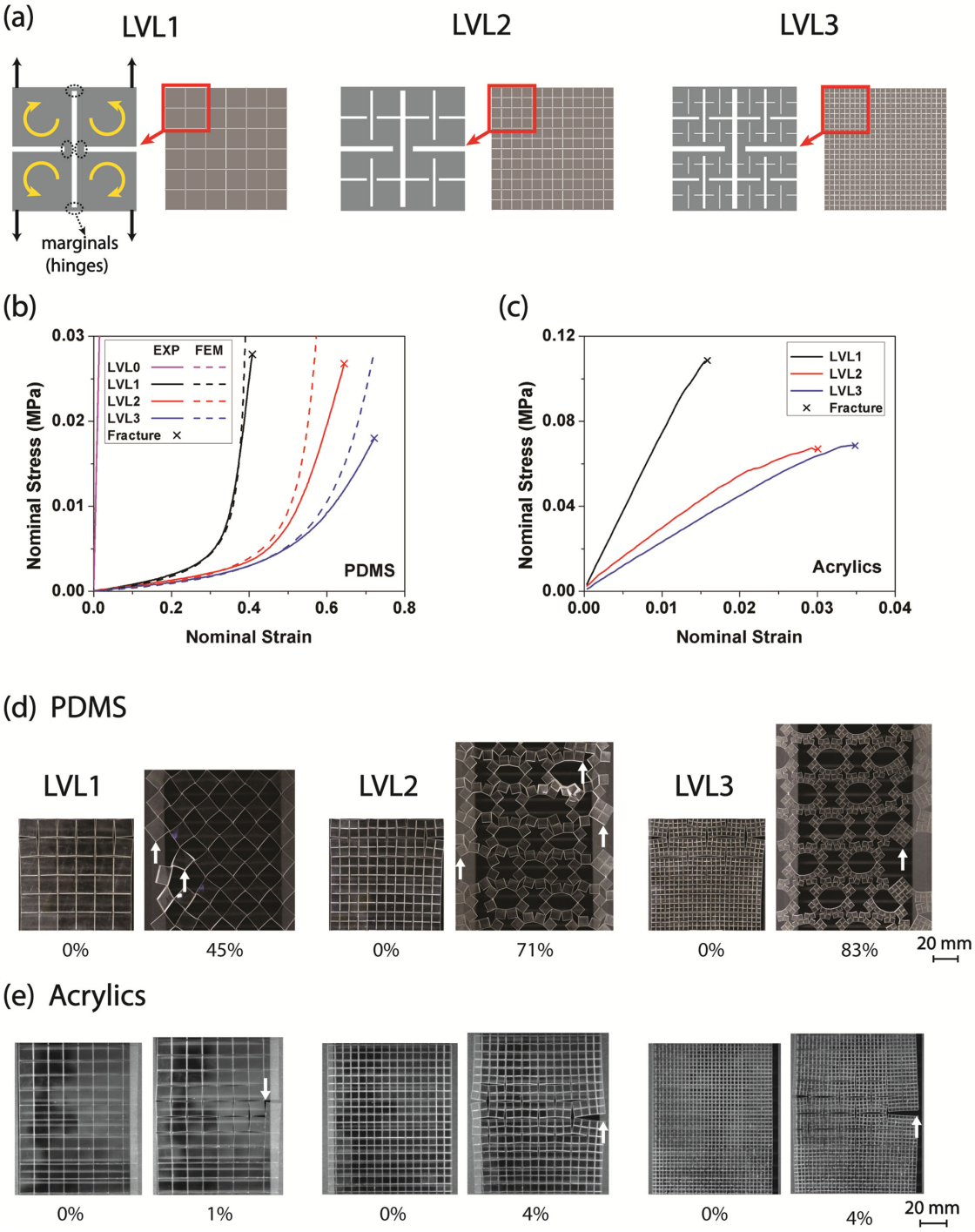

Figure 1. Mechanical behaviors of thin sheet of superelastic materials (PDMS) and brittle materials (Acrylics) with prescribed hierarchical cuts under uniaxial stretching. a) Schematic illustration of hierarchical line cuts (marked by white lines) in a representative square unit from Level 1 to Level 3. The cut square subunits are connected by uncut marginal at their corners, forming hinges. Upon uniaxial stretching, the subsquares undergo rotations around the marginal/hinge to expand biaxially, forming a periodic array of porous structures. Measured nominal stress–strain curves of the discrete structures until the hinge breaks in b) PDMS and c) Acrylics, the corresponding FEM simulation results are represented by dashed lines. Optical images of hierarchically cut d) PDMS and e) Acrylics samples before deformation and after rupture.

due to the far less stretchable characteristics of brittle materials. Figure 1c shows that the hinges break in Level 1 cuts at a very small strain for all levels ($\varepsilon_{f1} = 1.5\%$ for Level 1 and $\varepsilon_{f3} = 3.5\%$ for Level 3), far less than that of its original continuous thin sheet without cuts (fracture strain is $\varepsilon_{f0} = 7.1\%$). Only the pores at the first level are slightly opened but no observation of unit rotation

induced pattern transformation (Figure 1e), leading to a linear stress–strain response (Figure 1c). It should be noted that the maximum stretching strain at the onset of fracture in Acrylics is far below the maximum geometrically permissible stretching strain ε_{max} in the idealized model, consisting of rigid rotating units in hierarchically cut structures (ε_{max} = 43% for Level 1 and ε_{max} = 79% for Level 3 structure) according to ref. [26] where the model does not consider real materials properties. This discrepancy clearly demonstrates that to apply the cut concept and realize the full potentials of hierarchical cutting mechanical metamaterials, it is critical to investigate the influence of materials properties. In turn, it will feedback new design strategies as we will present in the following discussion.

The highly nonlinear and strain hardening behavior of the soft PDMS metamaterials with hierarchical cuts shown in Figure 1b is similar to that of hyperelastic materials, which can be well characterized using a third order Ogden hyperelastic model represented by dashed lines in **Figure 2**a (Figure S3, Supporting Information). Hyperelastic materials are described in terms of a strain energy potential U. For Ogden model, the general strain energy potential U_{Ogden} is given by:[40]

$$U_{Ogden}=\sum_{i=1}^{N}\frac{2\mu_i}{\alpha_i^2}\left(\bar{\lambda}_1^{\alpha_i}+\bar{\lambda}_2^{\alpha_i}+\bar{\lambda}_3^{\alpha_i}-3\right)+\frac{1}{D}(J-1)^2 \quad (1)$$

where $\bar{\lambda}_i=J^{-1/3}\lambda_i$ are the deviatoric stretches and $J=\lambda_1\lambda_2\lambda_3$ is the volume ratio. μ_i, α_i, and D are material constants fitted in the stress–strain curve, e.g., D is the inverse of bulk modulus. The initial shear modulus μ_0 and bulk modulus K_0 follow as $\mu_0=\sum_{i=1}^{N}\mu_i$ and $K_0=2/D$ for small strains. By taking $N=3$, i.e., the third order and fitting the Ogden potential to the uniaxial stress–strain curve over the whole strain range, the obtained material parameters are summarized in **Table 1**. The initial Young's modulus decreases from E_1 = 4.3 kPa (LVL 1) to E_3 = 1.3 kPa (LVL 3), the value of which at Level 3 is close to that of human skin (≈2 kPa).[35] Compared to that of continuous PDMS thin sheet without cuts (E_0 = 2.1 MPa), the initial Young's modulus in the cut structures drops approximately by 500 and 1600 times for Level 1 and Level 3, respectively. It can be envisioned that the Young's modulus will continue to drop significantly with the increasing level of cuts in the structure, leading to extremely compliant structures. The information of over one order stiffness decrease after cuts could provide important implication for design of ultra-soft materials to mimic human skin as well as conformable extremely soft substrate for bio-integrated electronics.[35] Furthermore, we perform cyclic loading/unloading tests of the hierarchical structures, which show an elastic and reversible mechanical response without any hysteresis (Figure S4, Supporting Information), further supporting the reversible reconfigurability of the metamaterials.

We believe that the highly nonlinear and hyperelastic stress–strain behavior observed in the hierarchical discrete structures is mainly originated from the cut structures, rather than the constituent hyperelastic material itself. Supporting this, Figure 2b shows nearly identical nonlinear stress–strain curves observed in the same structure made from two distinct material systems: one is linear elastic with Young's modulus of 2 MPa and Poisson's ratio of 0.49; and the other is highly nonlinear hyperelastic with initial Young's modulus of 2 MPa and Poisson's ratio of 0.49. Similarly, the nonlinear stress–strain curves from linear elastic constituent materials can also be well characterized with Ogden models (Figure S5, Supporting Information). Therefore, we refer the hierarchically cut structures as soft metamaterials.

To quantitatively understand the observed rupture in hierarchically cut PDMS and Acrylic structures, we analyze the stress distribution in the structures through both FEM simulations using the measured material properties and mapping of the strain distribution experimentally through digital image correlation (DIC). **Figure 3**a shows the corresponding simulated principal stress contours of hierarchically cut PDMS structures at the same stretching strain of ε = 40%. Severe stress concentration is observed at all hinge areas (highlighted with red color), and the highest stress concentration occurs in the hinges of Level 1 cut for all the structures, resulting in the first rupture of Level 1 hinges observed in experiments (Figure S2, Supporting Information). The reason for the observed severe stress concentration at Level 1 hinge is due to the fact that the higher level structural deformation cannot occur independently from the Level 1 deformation as revealed by Gatt

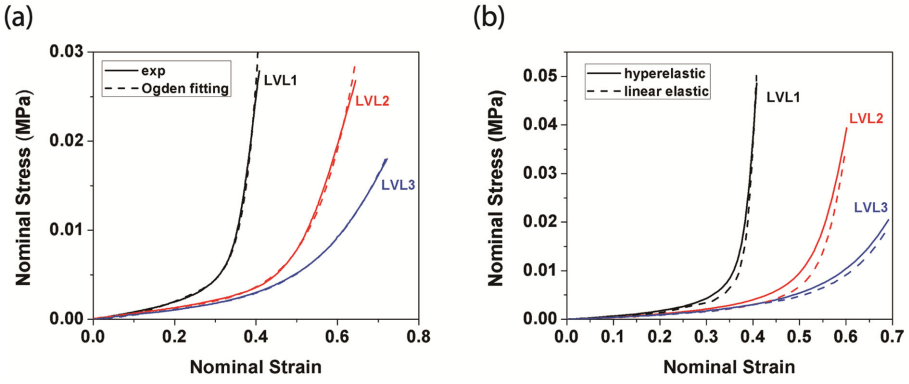

Figure 2. a) Experimentally measured stress–strain curves of hierarchically cut PDMS structures using third order Ogden hyperelastic model fitting. b) Simulated nominal stress–strain curves of the same hierarchical structures consisting of two different constituent materials: one is hyperelastic and the other is linear elastic with the same initial Young's modulus.

Table 1. Summary of fitted material parameters for structures from Level 1 to Level 3.

Parameters	Level 0	Level 1	Level 2	Level 3
(μ_1, μ_2, μ_3) [kPa]	(−454.7, 372.3, 792.9)	(−53.74, 49.04, 6.14)	(−44.36, 44.40, 2.52)	(28.12, 2.21, −29.92)
$(\alpha_1, \alpha_2, \alpha_3)$	(2.99, 5.79, −1.06)	(24.8, 25, 21.4)	(16.4, 16.4, 0.43)	(−7.6, 8.9, −10)
$\mu_0 = \sum_{i=1}^{3} \mu_i$[kPa]	710.5	1.44	2.56	0.41

et al.,[27] i.e., higher-level small square subunits can rotate only if the Level 1 hinges start to rotate and deform. This is also consistent with the observation from our FEM simulation, where the pores at Level 1 open first, followed by the pore opening at the higher levels. Under an extreme condition, for the rigid rotating model, if the Level 1 hinges were not allowed to rotate and deform, then the entire structure would be effectively "clamped" and cannot deform even though the higher level hinges could deform.[27] Thus, the deformation of Level 1 hinges is key to the overall structural deformation, thus bearing the highest stress concentration.

As the hierarchical level increases, under the same applied strain, the maximum principal stress in the hierarchical structure drops significantly (Figure 3b). By assuming the simple local failure criteria of maximum principal stress σ_{max_p} in an elastomer material, i.e., the rupture occurs when σ_{max_p} reaches the uniaxial tension strength, we observe that the increase in the hierarchy level leads to an enhanced fracture strain given the same measured ultimate tensile strength (represented by the dashed line in Figure 3b). The FEM simulation result is consistent with the observation in experiments (Figure 1b). Figure 3c shows that the maximum principal stress/strain is located in the inner circular arch of laser-cutter attributed U-shaped notch (see optical image in Figure S6, Supporting Information) as illustrated in Figure 3c, which is validated by the visualized strain contour using DIC measurements. It should be noted that despite the nearly identical nominal stress–strain curves as shown in Figure 2b for different elastic materials, Figure S7 (Supporting Information) shows that the maximum principal stress for constituent linear elastic material[26] is nearly twofold lower than that for the highly nonlinear material studied here. This implies that when real elastomeric material is modeled as a simplified linear elastic material rather than a hyperelastic one such as the case reported by Cho et al.,[26] it will largely underestimate the maximum principal stress the real structure undergoes in the hinges, especially at a relatively large applied stretching strain. Thus, without taking into account the real strength of elastomeric materials, the maximum expandability over 800% aerial coverage of the original area at a stretching strain of ≈1.8 is largely overestimated by Cho et al.[26] based on simplified linear elastic modeling of elastomers.

To enhance the mechanical strength of hierarchical cut metamaterials, thus the expandability of the 2D sheet, especially for those not so stretchable constituent materials, the key is to reduce the highest stress concentration located in the first level hinges. To do so, we can employ two general strategies, that is: i) rational design of the local shape of the first level hinges, and ii) design of the overall structure to allocate the loading at the first-level hinges to more hinges at a higher level.

As one of the examples in design of the local shape of a cut, a modified dog-bone-like hinge demonstrates superior performance by largely reducing the stress concentration within the hinges in comparison to the regular U-shaped notch as demonstrated in Figure 3d–f. At the same applied strain of 18%, FEM simulation shows that the maximum principal strain from the dog-bone-like hinge can be effectively reduced by approximately half versus that from the regular U-shaped hinge (Figure 3d), which holds true at further stretching. The DIC measurements on the contours of principal strains are consistent with the simulation. The stress concentration is largely reduced by increasing the load bearing area, as well as migrating the maximum stress from the notch apex to the two neighboring semicircles. Figure 3e shows the comparison of the normalized maximum stress $\bar{\sigma}_{max\_s}$ between different hinge shapes at the same stretching strain of 25% through simulation. By comparing the first three columns for a U-shaped notch with radius of r and hinge width d (the top row of Figure 3c), it is clear that increasing the ratio of r/d reduces the stress concentration,[40] where enlarging r increases the area of the hinge to distribute the load more evenly and decreasing d reduces the maximum stress under bending moment of M. Figure 3e further shows that the hinge shape could have a significant influence on $\bar{\sigma}_{max\_s}$, where the maximum principal stress in the U-shaped hinge with ($r/a = 0.005$ and $d/a = 0.05$) could be reduced more than 15 times using a dog-bone-like hinge ($r'/a = 0.05$, $d'/a = 0.05$). As proof-of-concept, we fabricate a plate with dog-bone-like cuts from brittle acrylics. As seen in Figure 3f, the fracture strain increases significantly, from 1.8% to 9% in Level 1 structure (Figure 3f). The enhanced fracture strain ($\varepsilon_{f1} = 9\%$) is even larger than its original continuous counterpart without cuts ($\varepsilon_{f0} = 7.1\%$). It should be noted that the dog-bone hinge shape could be further optimized to maximize the reduction of the stress concentration, and thus further enhance the fracture strain in the brittle materials.

In addition to the design of local hinge shape, the maximum principal stress in the hierarchically cut structure can also be reduced by: i) increasing the level of the hierarchical cuts as demonstrated in Figure 3b, and ii) modifying the cuts with linearly decreased hinge width. For hierarchically cut structures with the number of hierarchical levels of n, the total number of the hinges N_{total} in a representative volume element (RVE) unit cell is given by:

$$N_{total} = \frac{4}{3}\left(4^n - 1\right) \tag{2}$$

which increases exponentially with n. For Level 1, 2, 3, and 4 structures, the total number of hinges is 4, 20, 84, and 340, respectively. At a relatively small strain, the square unit is

ADVANCED MATERIALS
www.advmat.de

www.MaterialsViews.com

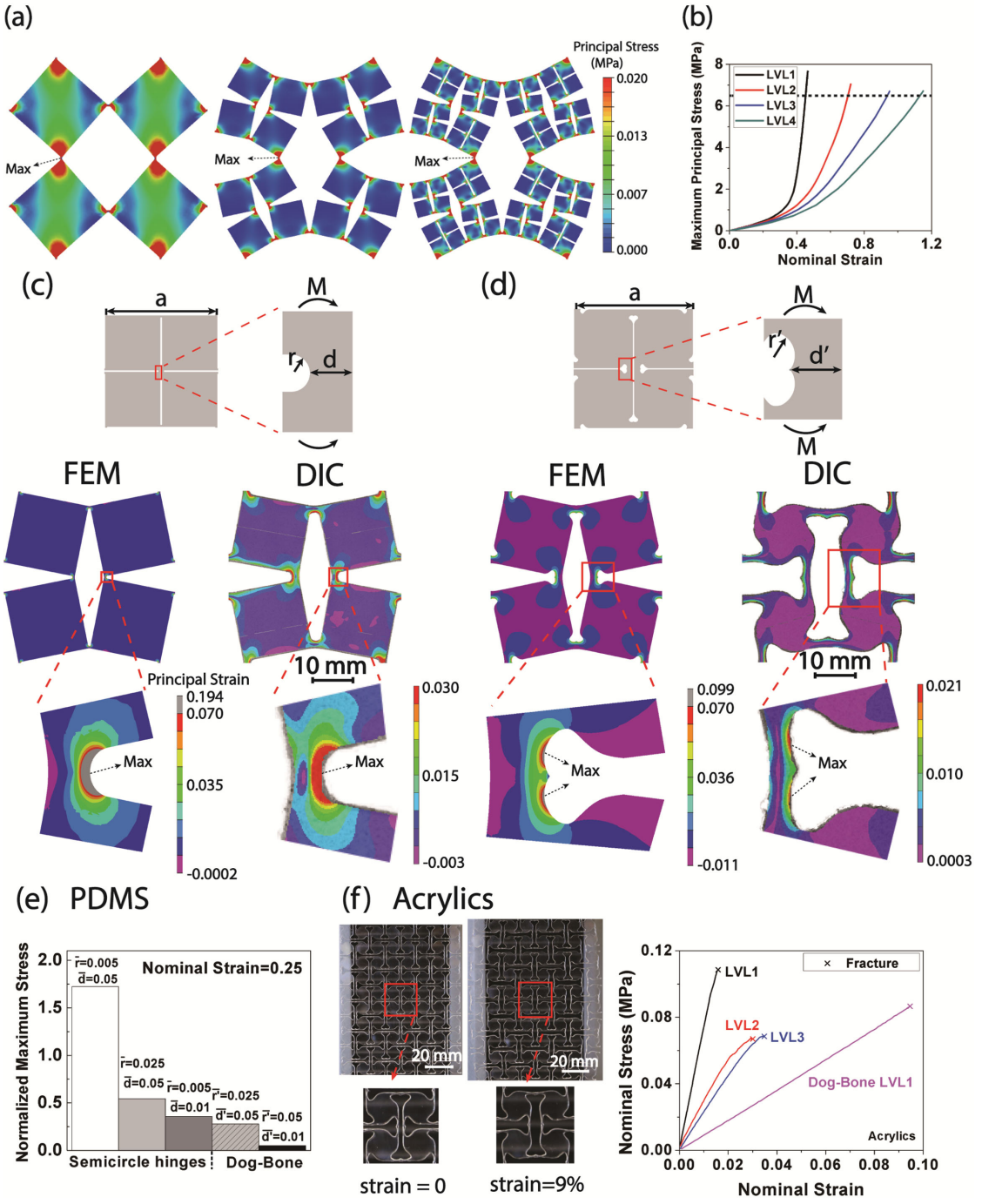

Figure 3. Design of local hinge shapes to improve the strength and stretchability of hierarchical cut structures. a) Simulated maximum principal stress contours of hierarchically cut PDMS samples show severe stress concentration in all the hinge area, leading to hinge rupture. b) Maximum principal stress as a function of applied nominal strain for cut PDMS structures from Level 1 to Level 4. The dashed line represents the ultimate tensile strength in PDMS materials. Numerical simulation and DIC measurement of the distribution of the principal strain in the PDMS thin sheets of c) regular laser cutter attributed U-shaped notch and d) modified dog-bone-like hinge shapes at a stretching strain of 18%, respectively. Level 1 units with different hinges obtained from a laser cutter are shown in schematics. e) Comparison of normalized maximum principal stress by initial Young's modulus in Level 1 PDMS structure with different sizes of U-shaped and dog-bone-like hinges. f) Left: optical images of Level 1 brittle Acrylics sheet with modified dog-bone-like hinges before and after uniaxial stretching. Right: Structures with dog-bone-like hinges show a superior stretchability and fracture strength than those with regular hinge shapes beyond 9% strain.

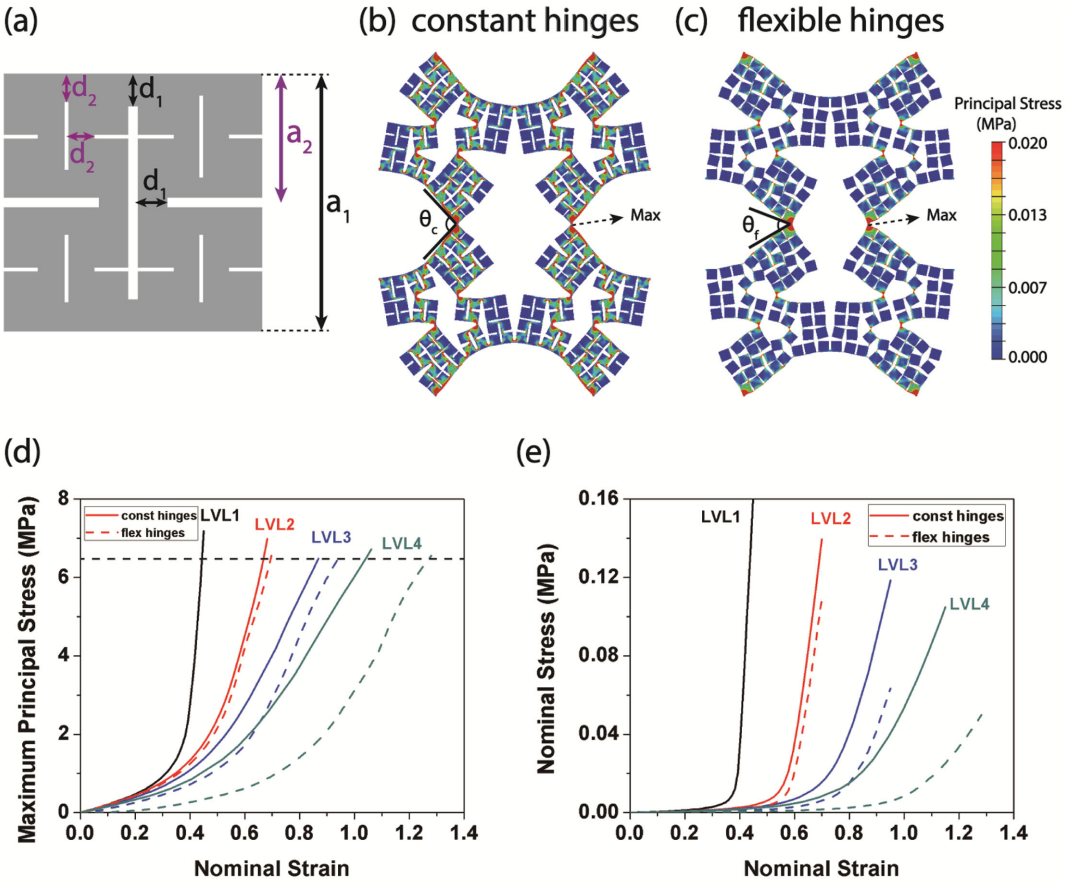

Figure 4. Design of global hierarchical hinge structures to enhance the strength and stretchability of hierarchical cut PDMS structures by more evenly distributing loading among all levels of bear-loading hinges. a) Schematic illustration of the structural designs with constant and flexible hinge width across all hierarchical levels in a representative unit cell. For constant hinge: $d_1 = d_2 = d_3 = ...d_n$; flexible hinges: the width decreases linearly with the increase of hierarchical levels, i.e., $d_1/a_1 = d_2/a_2 = d_3/a_3 = ...d_n/a_n$. Comparison of simulated principal stress contours in the same Level 4 structures with b) constant and c) flexible hinge distributions at a stretching strain of 70%, where they have the same hinge width at Level 1. d) Comparison of maximum principle stress in hierarchical structures with respective constant and flexible hinges as a function of nominal strain. e) Comparison of stress–strain curves in hierarchical structures with respective constant and flexible hinges.

nearly stress-free and can be considered as a rigid unit and all the loading is distributed to the load-bearing hinges. Generally speaking, the larger the number of hinges, the less the bearing load in the hinges on average. Therefore, the maximum principal stress is significantly reduced with the increase of hierarchical level as shown in Figure 3b, especially at large strains.

Next, we show that by setting the hierarchical cuts with flexible hinge width (see **Figure 4**a), which decreases linearly with the increase in the cut level, the maximum principal stress can be significantly reduced. Figure 4b,c shows the comparison of simulated maximum principal stress contour of Level 4 PDMS cut structure with constant (Figure 4b) and flexible hinge width (Figure 4c) at the same stretching strain of 70%. It shows that even with the same hinge width in the Level 1 cut, the opening angle θ_f in the structure with flexible hinge width (Figure 4b) is much smaller than that of θ_c with constant hinge width (Figure 4c), leading to substantial reduction in the maximum principal stress when compared to structures with constant hinge width. Thus, a large increase in the tensile strength of hierarchical cut structures is obtained (over 30% increase for Level 4 and more increased strength for a higher level), especially at a level higher than 3, as shown in Figure 4d. This is because that upon loading, the larger the number of hinges with narrower width in the subsquare units is, the more susceptible it is to deformation than the structure with constant hinge width. So the narrow hinges at higher cut levels can bear the load earlier and more load than hinges with constant width, which is harder to open at the higher cut level. Thus, it largely reduces the load bearing of Level 1 hinges, rendering the smaller opening angle at Level 1, and the structure becomes more complaint as observed in Figure 4e.

Through the combination of the aforementioned two strategies, we are confident that the simple hierarchical cut method could lead to extremely stretchable and expandable soft metamaterials, even from the least stretchable brittle materials, while attaining strength significantly higher than the original continuous structure.

Finally, we explore the potential application of such continuously reconfigurable metamaterials, which can tune phononic wave propagation and filter specific bands of frequencies, by simply control of mechanical strain induced pattern

transformation. Bloch-wave analysis is conducted using FEM to compute the phononic band structure of the hierarchical PDMS metamaterials at different level of macroscopic strains, where the normalized frequency is defined as $\tilde{\omega} = \omega A_0/2\pi C_T$ with A_0 being the original RVE square unit length. $C_T = \sqrt{\mu/\rho}$ is the transverse plane wave velocity in the homogeneous material. For PDMS, the initial shear modulus $\mu = 0.7$ MPa and its density $\rho = 1080$ kg m^{-3} so that $C_T = 24.8$ m s^{-1}.

Figure 5a–c shows the comparison of numerically calculated band diagrams between soft metamaterials with fractal cuts from Level 1 to Level 3 at the same representative stretching strain by normalized fracture strain ε_f, $\bar{\varepsilon} = \varepsilon/\varepsilon_f = 0$ (before deformation) and 1 (before rupture), respectively, where phononic bandgaps of forbidden frequencies are denoted by the gray filled area that in-plane waves could not propagate through. The evolution of the bandgap range as a function of the stretching nominal strain ε is shown in Figure 5d–f. The pattern transformation in Level 1 structure is equivalent to that in holy slabs,[18] where certain original bandgaps close and new bandgaps are formed during deformation (Figure 5d) through mechanical strain.[17] However, the introduction of hierarchical cuts shows a more complex bandgap structure and wider range of bandgap tunability that are not possible in Level 1 cut structure and simple periodic porous structures, especially at a lower frequency range due to its more complex shape shifting. Before deformation, when a higher level of cuts is introduced, the original high forbidden frequency of 0.08–0.42 in Level 1 structure (Figure 5d) is shifted to a lower frequency band of 0.01–0.22 in Level 2 (Figure 5e), and to 0.005–0.118 in Level 3 cut structure (Figure 5f). The higher the hierarchical level is, the lower frequency of bandgap it will generate, thus, more separate bandgaps at a lower frequency will be formed. After deformation, unlike the minor tunability of forbidden frequency filter in Level 1 cut structure as shown in Figure 5d (where the width of most bandgaps nearly remains unchanged with the increase of strain), the applied strain has a more pronounced influence on the evolution of bandgap structures for higher levels of hierarchically cut structures

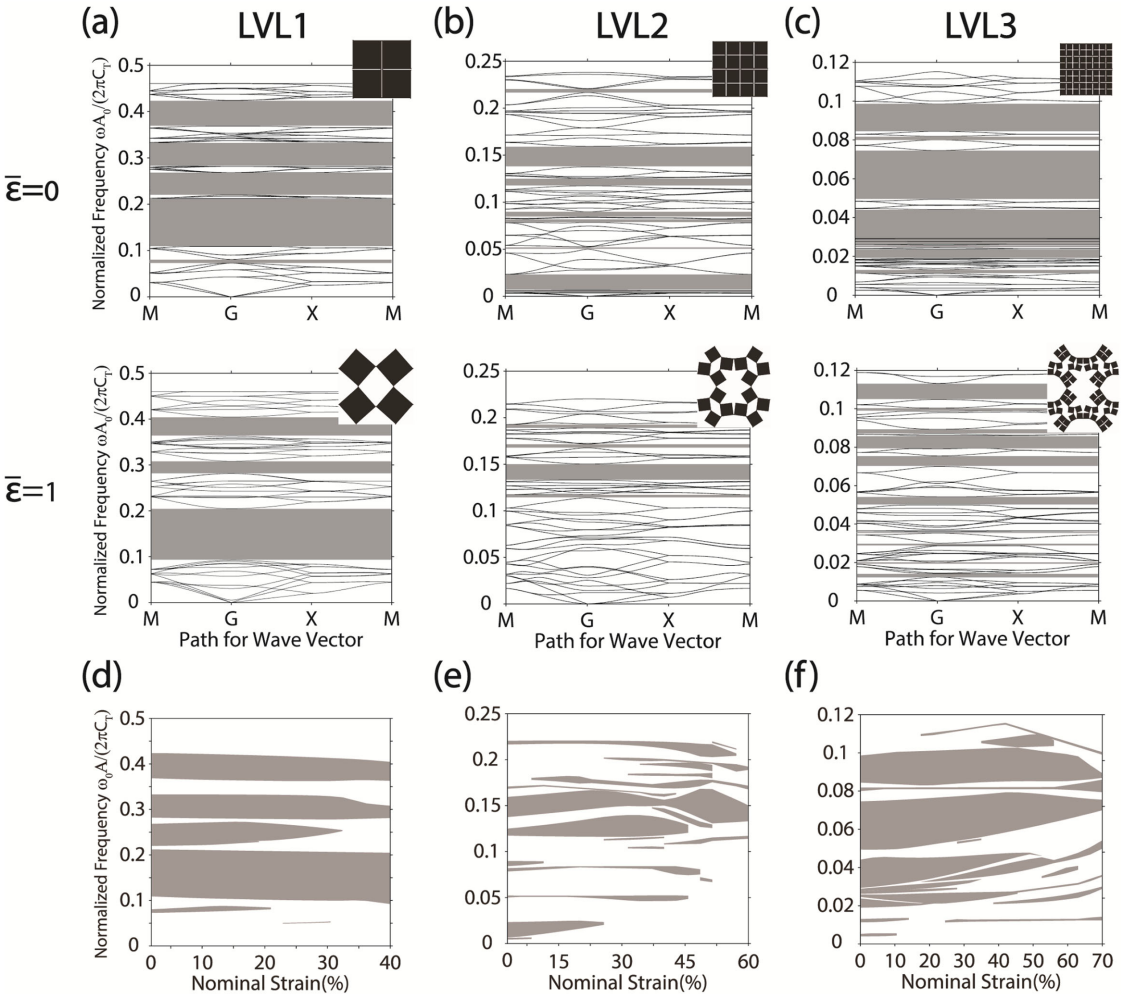

Figure 5. Tunable phononic bandgaps through deformation induced structure reconfiguration controlled by mechanical stretching strain in the hierarchically cut PDMS structures. a–c) Calculated phononic bandgaps in structures from Level 1 to Level 3 before deformation (top row) and at the onset of fracture (second row), and ε_f is the respective measured fracture strain in Figure 1b. Inset: the deformed lattice structures. The evolution of the calculated phononic bandgap map as a function of the stretching strain ε for the hierarchical metamaterials at d) Level 1, e) Level 2, and f) Level 3.

due to their more complex pattern transformation, as well as higher strength for larger stretchability. As the applied strain increases, the width of most original bandgaps before deformation in both Level 2 and 3 cut structures will narrow down dramatically and most bandgaps shift up to a higher frequency (Figure 5e,f). In addition, more new bandgaps are open within the higher frequency range in Level 2, whereas for Level 3 new bandgaps are open within its lower frequency range. We envision that the bandgap of hierarchically cut structures can be further tuned through control of either homogenous or heterogeneous distribution of hinge width across hierarchical levels for filter specified low-frequency acoustic waves.

In conclusion, by taking into account of the real material properties of the constituent materials, we study the mechanical behaviors of hierarchically cut soft metamaterials. We investigate the stress–strain behaviors as a function of structure, bending- versus stretching-dominated deformation mode upon stretching of the metamaterials. By comparing experiments and finite element simulation, we reveal the origin of structure failure. Through rational design of the geometrical shape of the local hinges and the global hierarchical cut structures and hinge width, we obtain extremely stretchable and highly expandable soft metamaterials with largely enhanced structure strength (both fracture strain and tensile strength) compared to the noncut sheets for both elastomers and brittle materials. They show a hyperelastic material behavior as a result of hierarchically cut structures rather than the constituent materials. We show that continuous and reversible structure reconfiguration without hysteresis allows for dynamic tuning of the phononic bandgap width and position, thus, filtering undesirable lower frequencies through simple mechanical strains by the control of hierarchical cut levels. The insights presented here will be critical to realize a broad range of potential applications of mechanical metamaterials, including tunable optics and acoustics,[41,42] scaffolds for conformable, stretchable electronics[32,37] and energy storage devices,[43] biomedical devices,[28] as well as foldable and deployable materials, with precisely controlled materials stiffness and mechanical response.

Experimental Section

Sample Fabrication: A thin PDMS sheet (≈80 mm long × ≈80 mm wide × ≈2 mm thick) was prepared from SYLGARD 184 silicone elastomer kit (Dow Corning) following the literature,[44] where the precursor and the curing agent were mixed at 10:1 weight ratio and cured at 70 °C in oven for 2 h. The prescribed hierarchical cuts were introduced into the sheet using a laser cutter (EPILOG LASER 40 Watts). The marginal width left by cuts was measured to be 0.188 ± 0.08 mm (mean value).

Uniaxial Tensile Test and DIC Measurement of Strain: Uniaxial tensile test was performed using Instron 5944 with a 2 kN load cell to characterize the stress–strain behaviors. The stress–strain curve was calibrated based on DIC measurements. The extension rate was 10 mm min^{-1}. Speckles were sprayed on the samples using an airbrush and India ink for DIC measurement. Images of the testing were taken at a rate of 1 fps (VicSnap, Correlated Solution) and DIC (Vic-2D, Correlated Solution) was used to track the deformation and obtain local strain contours.

FEM Simulation on Mechanical Response and Phononic Bandgap Calculation in PDMS: PDMS was modeled as a hyperelastic material (a third order Ogden model) with its materials parameters fitted according to experimental data (Figure S3a, Supporting Information), where the measured initial shear modulus is $\mu_0 = 0.71$ MPa and the bulk modulus is $K_0 = 35.3$ MPa. The mechanical response of hierarchical metamaterials was simulated using ABAQUS/Standard considering nonlinear effects of large displacements. An RVE of one square unit with hierarchical cuts was used to represent the periodic hierarchical structures with applied periodic boundary condition, where the thin cut sheet was modeled with plane-stress elements and locally refined mesh was applied to the uncut marginal to ensure the accuracy. The mesh density was validated from mesh convergence studies (see the Supporting Information for more details). Bloch-wave analysis was conducted using FEM software COMSOL Multiphysics 4.4 to compute the phononic band structure (see the Supporting Information for more details).

Supporting Information

Supporting Information is available from the Wiley Online Library or from the author.

Acknowledgements

S.Y. acknowledges the support from National Science Foundation (NSF)/ Polymer Program (No. DMR-1410253). L.H. acknowledges the funding support from the start-up grant at Drexel University. J.Y. acknowledges the funding support from the start-up at Temple University. The authors thank the helpful discussion with Dr. Lifeng Wang at Stony Brook University.

Received: May 29, 2015
Revised: September 7, 2015
Published online: October 13, 2015

[1] J.-H. Lee, J. P. Singer, E. L. Thomas, *Adv. Mater.* **2012**, *24*, 4782.
[2] Q. Zhao, L. Kang, B. Du, B. Li, J. Zhou, H. Tang, X. Liang, B. Zhang, *Appl. Phys. Lett.* **2007**, *90*, 011112.
[3] K. Bi, Y. Guo, X. Liu, Q. Zhao, J. Xiao, M. Lei, J. Zhou, *Sci. Rep.* **2014**, *4*, 4139.
[4] I. V. Shadrivov, P. V. Kapitanova, S. I. Maslovski, Y. S. Kivshar, *Phys. Rev. Lett.* **2012**, *109*, 083902.
[5] J. Y. Ou, E. Plum, L. Jiang, N. I. Zheludev, *Nano Lett.* **2011**, *11*, 2142.
[6] S. Babaee, J. Shim, J. C. Weaver, E. R. Chen, N. Patel, K. Bertoldi, *Adv. Mater.* **2013**, *25*, 5044.
[7] A. D. Boardman, V. V. Grimalsky, Y. S. Kivshar, S. V. Koshevaya, M. Lapine, N. M. Litchinitser, V. N. Malnev, M. Noginov, Y. G. Rapoport, V. M. Shalaev, *Laser Photonics Rev.* **2011**, *5*, 287.
[8] J. P. Turpin, J. A. Bossard, K. L. Morgan, D. H. Werner, P. L. Werner, *Int. J. Antennas Propag.* **2014**, *2014*, 18.
[9] A. Q. Liu, W. M. Zhu, D. P. Tsai, N. I. Zheludev, *J. Opt.* **2012**, *14*, 114009.
[10] A. C. Steven, S. David, *New J. Phys.* **2007**, *9*, 45.
[11] S. Zhang, L. Yin, N. Fang, *Phys. Rev. Lett.* **2009**, *102*, 194301.
[12] J. Mei, G. Ma, M. Yang, Z. Yang, W. Wen, P. Sheng, *Nat. Commun.* **2012**, *3*, 756.
[13] X. Zheng, H. Lee, T. H. Weisgraber, M. Shusteff, J. DeOtte, E. B. Duoss, J. D. Kuntz, M. M. Biener, Q. Ge, J. A. Jackson, S. O. Kucheyev, N. X. Fang, C. M. Spadaccini, *Science* **2014**, *344*, 1373.
[14] J. Paulose, B. G.-G. Chen, V. Vitelli, *Nat. Phys.* **2015**, *11*, 153.
[15] G. Wu, Y. Cho, I.-S. Choi, D. Ge, J. Li, H. N. Han, T. Lubensky, S. Yang, *Adv. Mater.* **2015**, *27*, 2747.
[16] M. Lapine, D. Powell, M. Gorkunov, I. Shadrivov, R. Marqués, Y. Kivshar, *Appl. Phys. Lett.* **2009**, *95*, 084105.
[17] K. Bertoldi, M. C. Boyce, *Phys. Rev. B* **2008**, *77*, 052105.

[18] B. Florijn, C. Coulais, M. van Hecke, *Phys. Rev. Lett.* **2014**, *113*, 175503.
[19] S. Rudykh, M. C. Boyce, *Phys. Rev. Lett.* **2014**, *112*, 034301.
[20] P. Wang, F. Casadei, S. Shan, J. C. Weaver, K. Bertoldi, *Phys. Rev. Lett.* **2014**, *113*, 014301.
[21] M. Schenk, S. D. Guest, *Proc. Natl. Acad. Sci. USA* **2013**, *110*, 3276.
[22] J. L. Silverberg, A. A. Evans, L. McLeod, R. C. Hayward, T. Hull, C. D. Santangelo, I. Cohen, *Science* **2014**, *345*, 647.
[23] T. Castle, Y. Cho, X. Gong, E. Jung, D. M. Sussman, S. Yang, R. D. Kamien, *Phys. Rev. Lett.* **2014**, *113*, 245502.
[24] M. K. Blees, A. W. Barnard, P. A. Rose, S. P. Roberts, K. L. McGill, P. Y. Huang, A. R. Ruyack, J. W. Kevek, B. Kobrin, D. A. Muller, P. L. McEuen, *Nature* **2015**, *524*, 204.
[25] T. C. Shyu, P. F. Damasceno, P. M. Dodd, A. Lamoureux, L. Xu, M. Shlian, M. Shtein, S. C. Glotzer, N. A. Kotov, *Nat. Mater.* **2015**, *14*, 785.
[26] Y. Cho, J.-H. Shin, A. Costa, T. A. Kim, V. Kunin, J. Li, S. Y. Lee, S. Yang, H. N. Han, I.-S. Choi, D. J. Srolovitz, *Proc. Natl. Acad. Sci. USA* **2014**, *111*, 17390.
[27] R. Gatt, L. Mizzi, J. I. Azzopardi, K. M. Azzopardi, D. Attard, A. Casha, J. Briffa, J. N. Grima, *Sci. Rep.* **2015**, *5*, 8395.
[28] J. N. Grima, R. Gatt, *Adv. Eng. Mater.* **2010**, *12*, 460.
[29] A. Slann, W. White, F. Scarpa, K. Boba, I. Farrow, *Phys. Status Solidi B* **2015**, *252*, 1533.
[30] S. Shan, S. H. Kang, Z. Zhao, L. Fang, K. Bertoldi, *Extreme Mech. Lett.* **2015**, DOI: 10.1016/j.eml.2015.05.002.
[31] L. Mizzi, K. M. Azzopardi, D. Attard, J. N. Grima, R. Gatt, *Phys. Status Solidi RRL* **2015**, *9*, 425.
[32] J. A. Rogers, T. Someya, Y. Huang, *Science* **2010**, *327*, 1603.
[33] J. Hu, L. Li, H. Lin, P. Zhang, W. Zhou, Z. Ma, *Opt. Mater. Express* **2013**, *3*, 1313.
[34] S. Wagner, S. P. Lacour, J. Jones, P.-H. I. Hsu, J. C. Sturm, T. Li, Z. Suo, *Physica E* **2004**, *25*, 326.
[35] K.-I. Jang, H. U. Chung, S. Xu, C. H. Lee, H. Luan, J. Jeong, H. Cheng, G.-T. Kim, S. Y. Han, J. W. Lee, J. Kim, M. Cho, F. Miao, Y. Yang, H. N. Jung, M. Flavin, H. Liu, G. W. Kong, K. J. Yu, S. I. Rhee, J. Chung, B. Kim, J. W. Kwak, M. H. Yun, J. Y. Kim, Y. M. Song, U. Paik, Y. Zhang, Y. Huang, J. A. Rogers, *Nat. Commun.* **2015**, *6*, 6566.
[36] J. N. Grima, K. E. Evans, *J. Mater. Sci. Lett.* **2000**, *19*, 1563.
[37] W. Yang, Z.-M. Li, W. Shi, B.-H. Xie, M.-B. Yang, *J. Mater. Sci.* **2004**, *39*, 3269.
[38] K. Bertoldi, P. M. Reis, S. Willshaw, T. Mullin, *Adv. Mater.* **2010**, *22*, 361.
[39] L. J. Gibson, M. F. Ashby, *Cellular Solids: Structure and Properties*, Cambridge University Press, Cambridge, UK **1999**.
[40] R. W. Ogden, *Proc. R. Soc. A* **1972**, *326*, 565.
[41] D. Shin, Y. Urzhumov, Y. Jung, G. Kang, S. Baek, M. Choi, H. Park, K. Kim, D. R. Smith, *Nat. Commun.* **2012**, *3*, 1213.
[42] J. N. Grima, R. Caruana-Gauci, M. R. Dudek, K. W. Wojciechowski, R. Gatt, *Smart Mater. Struct.* **2013**, *22*, 084016.
[43] K. Xie, B. Wei, *Adv. Mater.* **2014**, *26*, 3592.
[44] J. Yin, J. L. Yagüe, D. Eggenspieler, K. K. Gleason, M. C. Boyce, *Adv. Mater.* **2012**, *24*, 5441.